Proceedings of IWHT2013
2013 International Workshop on Heat Transfer Advances for Energy Conservation and Pollution Control
October 18-21, 2013, Xi'an, China

IWHT2013-084

Improved Treatment of Anisotropic Scattering in Radiative Transfer Analysis using the Finite Volume Method

Brian Hunter, Zhixiong Guo*
Department of Mechanical and Aerospace Engineering
Rutgers, The State University of New Jersey
98 Brett Road, Piscataway NJ, 08854
*corresponding Author: guo@jove.rutgers.edu

ABSTRACT

The impact of angular false scattering errors due to a lack of asymmetry factor conservation after FVM discretization is analyzed for radiative transfer in a cubic enclosure housing a highly-anisotropic participating medium. While the commonly implemented solid-angle splitting technique for phase-function treatment in the FVM is able to accurately conserve scattered energy in the system, errors in discretized phase-function asymmetry factor manifest, even for extremely fine splitting. A phase-function normalization technique introduced previously by the authors is applied to the 3-D FVM for the first time to improve treatment of anisotropic scattering by reducing angular false-scattering errors. Radiative transfer predictions generated using the FVM are compared to Monte Carlo (MC) and DOM predictions to gauge accuracy, as well as the necessity of proper phase-function normalization. Additional options of limiting angular false scattering, such as increases in direction number, are examined. While the flexibility of the FVM's directional quadrature allows for significant reduction in angular false-scattering errors without requiring phase-function normalization, increase in both direction number and solid-angle splitting adversely impacts computational efficiency. FVM radiative transfer predictions generated using the authors' normalization technique conform accurately to MC and DOM without substantial impact on computational resources.

[**Keywords:** Finite Volume Method, anisotropic scattering, phase-function normalization, radiative heat transfer]

INTRODUCTION

Numerical methods have recently garnered much attention in the field of radiation heat transfer with the advent of high-powered computational workstations, as they provide cost-effective and accurate alternatives to costly experimentation [1,2] In applications where radiation is the dominant mode of heat transfer, such as high temperature combustion and material processing [3-6], crystal growth [7], and laser-tissue interactions [8-10], accurate and complete solutions of the Equation of Radiative Transfer (ERT) are required for full radiation characterization. The integro-differential nature of the ERT makes it difficult to solve analytically, and thus numerical methods are preferred in order to accurately predict radiative transfer. One of the more common numerical methods for solving the ERT is the Finite Volume Method (FVM).

The FVM was introduced as a method of predicting radiative heat transfer by Raithby and Chui [11] around 1990, where the formulation for ERT solution was presented and verified via benchmark problems. Works by Chui and co-authors [12-14] determined radiative transfer in both axisymmetric and non-axisymmetric cylindrical enclosures using the FVM with non-orthogonal meshes [13] and for applications involving pulverized fuel flames [14]. Murthy and Mathur [15] and Kim et al. [16] determined radiative transfer using the FVM in two-dimensions using unstructured meshes.

Chai et al. [17] extended the FVM to determine radiative transfer in 3-D enclosures containing participating media, investigating the impact of collimated incidence and heat generation. Raithby [18] presented a discussion of the FVM in 2- and 3-D enclosures with unstructured grids, comparing predictions to those determined using the DOM. Baek et al. [19] determined radiative transfer in a kidney-shaped, 3-D combustion chamber using non-orthogonal meshes, determining that the FVM was a moderately efficient method. Seung et al. [20] assessed the FVM and DOM for radiative heat transfer in a 3-D rectangular enclosure, finding good agreement between both methods. Chai et al. [21] analyzed ultrafast radiative heat transfer in a 3-D rectangular medium using the

FVM, expanding on an earlier similar analysis using the DOM by Guo and Kumar [22]. Kim and Huh [23] introduced a new angular discretization scheme for the FVM, determining radiative transfer in a 3-D anisotropically scattering media and comparing results with Monte Carlo predictions. Additional works by Borjini et al. [4] and Kamel et al. [24] used the 3-D FVM to determine radiative heat transfer in a baffled combustion chamber containing a non-gray sooting media.

In many practical applications involving participating media, scattering is anisotropic. In all discretization-based numerical methods including FVM and DOM, the continuous angular variation is approximated using a finite number of discrete radiation directions. A well-known issue stemming from said angular discretization for anisotropically scattering media is that scattered energy becomes non-conserved after directional discretization [25]. For the DOM, non-conservation of scattered energy is corrected using phase-function normalization [26], which has been shown recently to lead to distortions in phase-function asymmetry factor [26-30], an error recently termed as "angular false scattering" [29,30]. For the FVM, scattered energy can be accurately conserved after directional discretization using solid-angle splitting [12]. Boulet et al. [26] claimed that phase-function normalization was not necessary for the FVM, due to the accurate satisfaction of the energy condition. However, Hunter and Guo [31] showed that angular false scattering errors still persisted after FVM discretization in a 2-D axisymmetric cylindrical enclosure, prompting additional treatment to correct such an issue.

Recently, Hunter and Guo [27-31] introduced a phase-function normalization technique, developed to simultaneously conserve scattered energy and phase-function asymmetry factor after directional discretization. The impact of said normalization on angular false scattering errors was analyzed for 2-D axisymmetric [27,28] and 3-D cubic enclosures [29,30] using the DOM, where DOM predictions were vastly improved in comparison to benchmark Monte Carlo results using said technique. Hunter and Guo [31] addressed the issue of angular false scattering errors using the FVM in 2-D axisymmetric cylindrical enclosures, finding that additional normalization is required even with substantial refinement in solid-angle splitting. However, as most practical applications cannot be approximated as two-dimensional, investigation of angular false scattering errors for 3-D radiative transfer using the FVM is necessary.

In this study, radiative transfer in a 3-D cubic enclosure containing an anisotropically scattering media is predicted using the FVM. The necessity of using authors' phase-function normalization technique to ensure the minimization of angular false-scattering errors and improve treatment of anisotropic scattering in radiative transfer analysis is presented. Heat fluxes generated using the FVM both with and without additional phase-function normalization are compared to MC results [26] and DOM results [30] to gauge the accuracy of the FVM predictions. The impact of solid-angle splitting on both energy and asymmetry factor conservation is analyzed. A discussion on the computational advantages of phase-function normalization over other methods of conserving scattering properties, such as substantial increase in FVM discrete directions, is presented.

NOMENCLATURE

$A^{l'l}$	Normalization coefficients
D_i^l	Directional weight at face i in direction l
g	Asymmetry factor
I	Radiative intensity ($W/m^2 sr$)
M	Total number of directions
N_ϕ, N_θ	Number of divisions in azimuthal and polar direction
$N_{s\phi}, N_{s\theta}$	Solid angle sub-divisions in azimuthal and polar direction
$\hat{\boldsymbol{n}}$	Surface outward unit normal vector
$\boldsymbol{r}$	Position vector
$\hat{\boldsymbol{s}}$	Unit direction vector

Greek Symbols

$\Delta A, \Delta V$	Control volume surface area and volume (m^2, m^3)
$\Delta\Omega$	Discrete solid angle (sr)
σ_a	Absorption coefficient (m^{-1})
σ_s	Scattering coefficient (m^{-1})
Φ	Scattering phase function
$\tilde{\Phi}$	Normalized scattering phase function
ϕ	Radiation direction azimuthal angle (°)
Θ	Scattering angle (°)
θ	Radiation direction polar angle (°)
ω	Scattering albedo, $= \sigma_s/(\sigma_a + \sigma_s)$

Subscripts

b	Blackbody
HG	Henyey-Greenstein
i	Control-volume face

Superscripts

$'$	Radiation incident direction
l, l'	Radiation directions
$l'l$	From direction l' into direction l

DISCRETIZATION OF ERT

The steady-state ERT of radiation intensity I in a gray, absorbing-emitting and anisotropically scattering medium can be expressed, using general vector notation, as follows:

$$\hat{\boldsymbol{s}} \cdot \nabla I(\boldsymbol{r}, \hat{\boldsymbol{s}}) = -(\sigma_a + \sigma_s) I(\boldsymbol{r}, \hat{\boldsymbol{s}}) + \sigma_a I_b(\boldsymbol{r}) + \frac{\sigma_s}{4\pi} \int_{4\pi} I(\boldsymbol{r}, \hat{\boldsymbol{s}}') \Phi(\hat{\boldsymbol{s}}', \hat{\boldsymbol{s}}) d\Omega' \quad (1)$$

In the preceding equation, the term on the left-hand side accounts for spatial gradients of radiative intensity, while the three right-hand side terms represent intensity attenuation due

to both absorption and radiative out-scattering, intensity augmentation due to blackbody emission, and intensity augmentation due to in-scattering of radiative energy, respectively.

Using a control-volume approach, Eq. (1) is integrated over an arbitrary control volume ΔV and discrete solid angle $\Delta\Omega^l$ [17], defined by azimuthal angle ϕ and polar angle θ, where the discrete radiation direction $\hat{\boldsymbol{s}}^{\boldsymbol{l}}$ denotes the centroid of $\Delta\Omega^l$ [15, 17, 21]. After performing the integration, Eq. (1) can be expressed as follows, for discrete direction $\hat{\boldsymbol{s}}^{\boldsymbol{l}}$:

$$\int_{\Delta\Omega^l}\int_{\Delta A} I^l(\hat{\boldsymbol{s}}^{\boldsymbol{l}}\cdot\hat{\boldsymbol{n}})dAd\Omega^l = \int_{\Delta\Omega^l}\int_{\Delta V}[-(\sigma_a+\sigma_s)I^l+S^l]dVd\Omega^l \tag{2}$$

where the volume integral on the left-hand side has been replaced by a surface area integral via Gauss' theorem [1,2]. Evaluation of the integrals in Eq. (2) over control volume and solid angle leads to the following discretized form for the ERT:

$$\sum_i I_i^l A_i D_i^l = -(\sigma_a+\sigma_s)I^l\Delta V\Delta\Omega^l + S^l\Delta V\Delta\Omega^l \tag{3}$$

where $l = 1,2,\dots,M$. The area integration of the spatial gradient term can be converted to a summation over the i faces of an arbitrary control volume, under the assumption that intensity at any location in a control volume and solid angle is equal to the mean intensity over said control volume and solid angle [15]. In this summation, I_i^l represents radiative intensity in discrete direction $\hat{\boldsymbol{s}}^{\boldsymbol{l}}$ at control-volume face i, A_i is the facial surface area of control-volume face i, and D_i^l is the directional weight of discrete direction $\hat{\boldsymbol{s}}^{\boldsymbol{l}}$ at control-volume face i, evaluated using the following expression:

$$D_i^l = \int_{\Delta\Omega^l}(\hat{\boldsymbol{s}}^{\boldsymbol{l}}\cdot\hat{\boldsymbol{n}}_{\boldsymbol{i}})\,d\Omega^l \tag{4}$$

where $\hat{\boldsymbol{n}}_{\boldsymbol{i}}$ is the unit vector normal to control-volume face i.

The source term S^l can be expressed as

$$S^l = \sigma_a I_b + \frac{\sigma_s}{4\pi}\sum_{l'=1}^{M}\bar{\Phi}^{l'l}\,I^{l'}\Delta\Omega^{l'} \tag{5}$$

where the radiative in-scattering integral in Eq. (1) has been approximated using a discrete quadrature summation. In this summation, $\bar{\Phi}^{l'l}$ is the average scattering phase function between two discrete solid angles $\Delta\Omega^{l'}$ and $\Delta\Omega^l$, which can be calculated as such:

$$\bar{\Phi}^{l'l} = \frac{1}{\Delta\Omega^{l'}\Delta\Omega^l}\int_{\Delta\Omega^l}\int_{\Delta\Omega^{l'}}\Phi(\hat{\boldsymbol{s}}',\hat{\boldsymbol{s}})d\Omega'd\Omega \tag{6}$$

The necessity of using an averaged scattering phase function will be described later.

Unlike the DOM, in which the choice of discrete directions is restricted due to the necessity of satisfying directional moments, the choice of directions for the FVM is generally arbitrary. Commonly, the total solid angle of $4\,\pi$ is approximated using $M = (N_\phi \text{ x } N_\theta)$ discrete directions, where N_ϕ and N_θ are the number of divisions in azimuthal and polar angle, respectively. However, Kim and Huh [23] discovered that, for 3-D problems, angular discretization in this manner can result in highly non-uniform solid angles. Additionally, this method of discretization can result in certain directions having zero direction cosines in one of the three ordinate directions, rendering that direction useless in a control-volume marching scheme.

To combat this issue, Kim and Huh [23] introduced a new angular discretization method for the FVM called the FT_N-FVM. Using this method, the total polar angle θ is divided into an even number N uniformly spaced directional levels. The number of azimuthal divisions corresponding to the N polar levels follows the arithmetic sequence $4, 8, 12, \dots 2N-4, 2N, 2N-4, \dots, 12, 8, 4$. The total number of directions becomes $M = N(N+2)$, identical to the number of directions in the DOM S_N quadrature. Kim and Huh [23] showed that not only does this procedure produce more uniform solid-angles, it also leads to radiative transfer results that are of equal or better accuracy than the commonly used $(N_\phi \text{ x } N_\theta)$ angular discretization for the FVM. To this end, the FT_N-FVM discretization procedure of Kim and Huh [23] is implemented for all forthcoming results in this analysis.

Additional details on the discretization of the ERT and solution procedure using the FVM are not presented here, for brevity, but are available in textbook [1] and references [28,32].

PHASE FUNCTION NORMALIZATION

When implementing numerical methods to solve the ERT, it is well established that discretization of the continuous angular variation must preserve scattered energy conservation in the system. In order to ensure the preservation of energy conservation after directional discretization, the following relation must hold for all discrete directions $\hat{\boldsymbol{s}}^{\boldsymbol{l}'}$:

$$\frac{1}{4\pi}\sum_{l=1}^{M}\Phi^{l'l}\Delta\Omega^l = 1 \tag{7}$$

If scattering is anisotropic, the above condition may not be explicitly satisfied [12]. Inaccurate conservation of scattered energy has been shown to produce inaccurate radiative transfer predictions [26].

To correct this issue, Chui and Raithby [12] introduced a solid-angle splitting technique, in which each solid angle $\Delta\Omega^l$ is sub-divided into multiple sub-angles $\Delta\Omega^{l_s}$. The total

scattered energy between any two arbitrary solid angles is then calculated by averaging the energy scattered between their corresponding sub-angles. Using this technique, the average scattering phase function of Eq. (6) can be approximated as follows [11]:

$$\bar{\Phi}^{l'l} \cong \frac{1}{\Delta\Omega^{l'}\Delta\Omega^{l}} \sum_{l_s=1}^{M_s} \sum_{l'_s=1}^{M'_s} \Phi^{l'_s l_s} \Delta\Omega^{l'_s} \Delta\Omega^{l_s} \tag{8}$$

In the preceding equation, $\Phi^{l'_s l_s}$ is the discrete scattering phase function between sub-angles $\Delta\Omega^{l'_s}$ and $\Delta\Omega^{l_s}$, and M_s and M'_s are the number of total sub-angles in solid angles $\Delta\Omega^{l}$ and $\Delta\Omega^{l'}$, respectively.

After averaging, the scattered energy conservation criterion of Eq. (7) can be expressed as

$$\frac{1}{4\pi} \sum_{l=1}^{M} \bar{\Phi}^{l'l} \Delta\Omega^{l} = 1 \tag{9}$$

Assuming every solid angle is divided into a sufficient number of sub-angles, this conservation condition will be accurately satisfied for all directions $\hat{\boldsymbol{s}}^{\boldsymbol{l'}}$, regardless of phase-function type.

In order to ease numerical computation, approximations to the highly-oscillatory Mie phase function Φ are commonly implemented, as the physical nature of Φ makes it difficult to efficiently adopt. For highly-anisotropic scattering, the Henyey-Greenstein (HG) phase function is widely accepted as a suitable approximation, due to its accurate representation of the strong forward-scattering peak [1,2]. The HG phase function approximation can be expressed as

$$\begin{aligned} \Phi_{HG}(\Theta) &= \sum_{n=0}^{\infty} (2n+1) g^n P_n(\cos\Theta) \\ &= \frac{1-g^2}{[1+g^2-2g\cos\Theta]^{1.5}} \end{aligned} \tag{10}$$

where Θ is the scattering angle between incoming and outgoing radiation directions, and the phase-function asymmetry factor g is the average cosine of scattering angle.

Figure 1 illustrates the dependence of scattered energy conservation on the number of solid angle sub-angles after FVM discretization. The continuous angular variation is discretized using M = 24, 48, 80, 168, and 288 discrete directions ($N = 4, 6, 8, 12, 16$). Each solid angle is sub-divided into ($N_{s\phi}$ x $N_{s\theta}$) sub-angles, with $N_{s\phi} = N_{s\theta}$, ranging from (2 x 2) to (24 x 24) divisions. Scattered energy conservation is presented for the HG phase function approximation with asymmetry factor g = 0.9300.

For a given number of directions M, increases in the number of sub-angles reduces the discrepancy in discretized scattered energy conservation. For low solid-angle splitting, significant deviations in scattered energy conservation are witnessed for all M, with larger deviations appearing for lower-order quadrature. In order to conserve scattered energy accurately within 0.001%, ($N_{s\phi}$ x $N_{s\theta}$) = (24 x 24), (20 x 20), (20 x 20), (12 x 12), and (12 x 12) sub-angles are required for M = 24, 48, 80, 168, and 288, respectively. The converging nature of the data in Figure 1 shows that sufficient solid-angle splitting will accurately conserve scattered energy after FVM discretization, without any additional treatment.

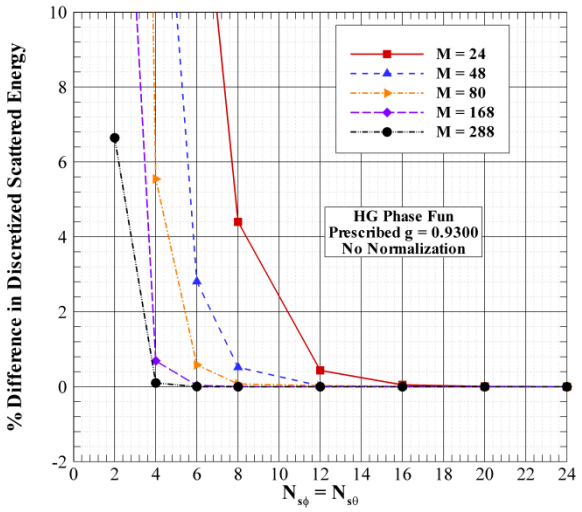

Figure 1: Deviation from scattered energy conservation versus solid angle splitting number for HG phase function with g = 0.9300 with various angular quadratures and no normalization

In addition to scattered energy conservation, the overall phase-function asymmetry factor g should also be conserved after directional discretization, in order to ensure that radiative properties of the original problem are not altered [27]. In order to ensure that the phase-function asymmetry factor is conserved, the following relation should hold for all discrete directions $\hat{\boldsymbol{s}}^{\boldsymbol{l'}}$:

$$\frac{1}{4\pi} \sum_{l=1}^{M} \bar{\Phi}^{l'l} \cos\Theta^{l'l} \Delta\Omega^{l} = g \tag{11}$$

where $\Theta^{l'l}$ is the scattering angle between incoming discrete direction $\hat{\boldsymbol{s}}^{\boldsymbol{l'}}$ and scattered direction $\hat{\boldsymbol{s}}^{\boldsymbol{l}}$.

For the same directional quadratures and solid-angle splitting levels as Figure 1, Figure 2 illustrates the deviation from asymmetry factor conservation for a g = 0.9300 HG phase function. For lower amounts of sub-angles, significant deviations from conservation are witnessed for all directional quadratures. However, instead of converging towards 0%

with significant increase in sub-angle number (as energy conservation did in Figure 1), the deviation from asymmetry factor conservation converges to a value less than the prescribed $g = 0.9300$. For $(N_{s\phi} \times N_{s\theta}) = (24 \times 24)$, the discretized asymmetry factors for $M = 24, 48, 80, 168$, and 288 attain values of $g = 0.8855$, 0.9024, 0.9113, 0.9198, and 0.9237, respectively, corresponding to percentage differences of -4.79%, -2.97%, -2.01%, -1.09%, and -0.68%. This discrepancy between prescribed and discretized asymmetry factor in the FVM had gone largely unnoticed, as the commonly implemented splitting technique was assumed to accurately conserve asymmetry factor [26] as well as scattered energy.

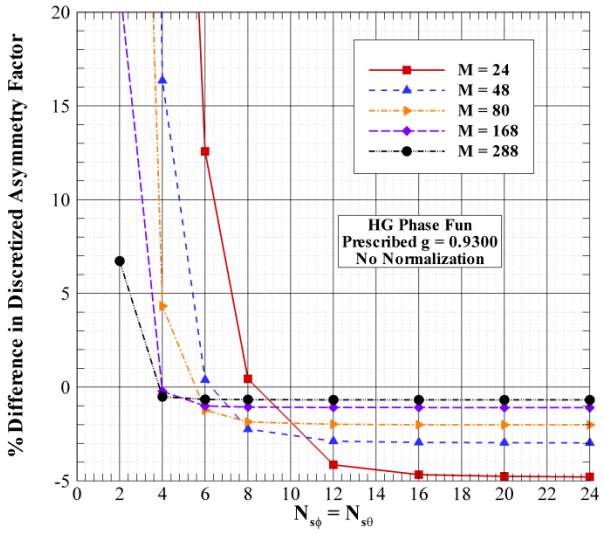

Figure 2: Deviation from asymmetry factor conservation versus solid angle splitting number for HG phase function with g = 0.9300 with various angular quadratures and no normalization

Increasing the number of directions does reduce the discrepancy between the prescribed asymmetry factor and discretized value at high splitting level, however small errors in discretized phase-function asymmetry factor can produce significant errors in radiative transfer predictions. Errors of this type have been recognized as a second type of false-scattering due to angular discretization, or "angular false-scattering" [29,30]. Hunter and Guo [30] recently investigated the impact of small deviations in phase-function asymmetry factor on angular false-scattering errors in the DOM for a 3D cubic enclosure, determining that even slight discrepancies in asymmetry factor can result in significant errors, since the change in overall scattering effect is manifested in the difference of $(1-g)$, according to the isotropic scaling law [33,34]. Angular false-scattering errors were shown to be significant mainly for highly-anisotropic scattering ($g \geq 0.80$). Thus, for highly anisotropic scattering in the FVM, additional phase-function treatment to ensure simultaneous satisfaction of Eq. (9) and Eq. (11) is required, as the commonly adopted splitting procedure to conserve Eq. (9) results in altered asymmetry factors for all quadratures.

Hunter and Guo [27-31] recently introduced a new phase-function normalization technique, fashioned to accurately conserve both scattered energy and phase-function asymmetry factor simultaneously. The average scattering phase function is normalized in the following manner:

$$\tilde{\Phi}^{l'l} = (1 + A^{l'l})\bar{\Phi}^{l'l} \tag{12}$$

where the normalization parameter $A^{l'l}$ corresponds to scattering between two discrete directions $\hat{\mathbf{s}}^{l'}$ and $\hat{\mathbf{s}}^{l}$. The normalized scattering phase function $\tilde{\Phi}^{l'l}$ is subject to the following constraints:

$$\frac{1}{4\pi}\sum_{l=1}^{M} \tilde{\Phi}^{l'l}\Delta\Omega^{l} = 1, \qquad l' = 1,2,\ldots,M \tag{13a}$$

$$\frac{1}{4\pi}\sum_{l=1}^{M} \tilde{\Phi}^{l'l}\cos\left(\Theta^{l'l}\right)\Delta\Omega^{l} = g, \qquad l' = 1,2,\ldots,M \tag{13b}$$

$$\tilde{\Phi}^{l'l} = \tilde{\Phi}^{ll'} \tag{13c}$$

where the first two constraints come from Eq. (9) and Eq. (11), and the third constraint is due to scattering directional symmetry. The system comprised of Eqs. (12-13) is underdetermined, and thus has infinite solutions. The solution with minimum error, called the minimum-norm solution, can be determined using pseudo-inversion, and will provide values of normalization parameter $A^{l'l}$ which will accurately conserve scattered energy as well as asymmetry factor after FVM discretization.

PHYSICAL RESULTS AND DISCUSSION

While Fig. (2) presents the mathematical reasoning behind applying phase-function normalization to ensure satisfaction of Eq. (11) after directional discretization, an analysis of radiative transfer results is required in order to determine the absolute necessity of such a treatment to reduce angular false-scattering errors. Hunter and Guo previously applied this technique for FVM radiative transfer analysis in a 2-D axisymmetric medium [31], however in most practical applications, such simplifications to two dimensions are not practical. Thus, it is important to investigate the impact of the deviations in asymmetry factor witnessed in Fig 2 and the importance of applying phase-function normalization for FVM radiative transfer analysis in a 3-D medium.

The computing workstation used for this analysis is a Dell Optiplex 780, with an Intel 2 Dual Core 3.16 GHz processor and 4.0 GB of RAM. The FVM procedure was implemented using the FORTRAN computing language, and the values of the normalization parameters were determined by using MATLAB, and imported into FORTRAN. Since the

normalization parameters depend solely on the quadrature scheme and phase function asymmetry factor, and not on the physical properties of the problem, they need only be determined once for a given phase function.

The benchmark test problem analyzed in this study involves radiative transfer in a cubic enclosure of edge length L which houses an absorbing-emitting and anisotropically scattering medium. The spatial coordinates are non-dimensionalized as follows: $x^* = x/L$, $y^* = y/L$, and $z^* = z/L$. The optical thickness and scattering albedo of the medium are $\tau = (\sigma_a + \sigma_s)L$ and $\omega = \sigma_s/(\sigma_a + \sigma_s)$. Unless otherwise specified, the medium is taken to be optically thick (τ = 10.0) and purely scattering (ω = 1.0). As a means of simplifying the analysis, the edge length of the cube is taken to be unity for all analyses. For all analyses, the medium is taken to be cold ($I_b = 0$). All boundary walls are black, with the wall at z^* = 0 taken as a diffuse emitter with unity emissive power, and all remaining walls are taken to be cold. In order to relate the intensities at control-volume nodes to that of the control-volume faces in the FVM solution scheme, the positive spatial differencing scheme is used.

An analysis of the spatial grid density is presented in Figure 3. The radiative heat flux Q is calculated along the centerline of the wall opposite from the diffuse source, i.e. $Q(x^*, y^* = 0.5, z^* = 1.0)$. The asymmetry factor of the medium is taken to be $g = 0.9300$. Solutions generated using the FVM with M = 168 discrete directions with $(N_{s\phi}$ x $N_{s\theta})$ = (12 x 12) solid-angle splitting are compared to reference Monte Carlo (MC) solutions [26] for varying spatial grid density. The MC results were computed with greater than 4 million quanta per control volume, with spatial grid $(N_x$ x N_y x $N_z)$ = (21 x 21 x 21). For the FVM results, the spatial grid was ranged between $(N_x$ x N_y x $N_z)$ = (7 x 7 x 7) and $(N_x$ x N_y x $N_z)$ = (27 x 27 x 27), in order to determine the grid density required to minimize error with further grid refinement. The FVM results were determined using Hunter and Guo's normalization of Eqs. (12)-(13).

For low grid density, significant errors are witnessed when comparing FVM solutions to MC. As spatial grid density is increased, FVM solutions begin to converge, with further grid refinement past $(N_x$ x N_y x $N_z)$ = (27 x 27 x 27) resulting in insignificant changes (less than 0.1%) in heat flux predictions. When compared with MC, it is seen that the FVM profiles converge to a heat flux that slightly underpredicts MC at all locations, with errors ranging between -4.62% and -1.06%. Errors of this magnitude between FVM and MC solutions are acceptable, due to both discretization error in the FVM and statistical error inherent in the MC. While the FVM with $(N_x$ x N_y x $N_z)$ = (17 x 17 x 17) spatial grid appears to conform most accurately to the MC, errors due to insufficient spatial discretization exist, and thus further refinement is necessary. According to this analysis, use of the $(N_x$ x N_y x $N_z)$ = (27 x 27 x 27) spatial grid will effectively minimize errors due to spatial discretization, and thus this grid will be implemented for all forthcoming results.

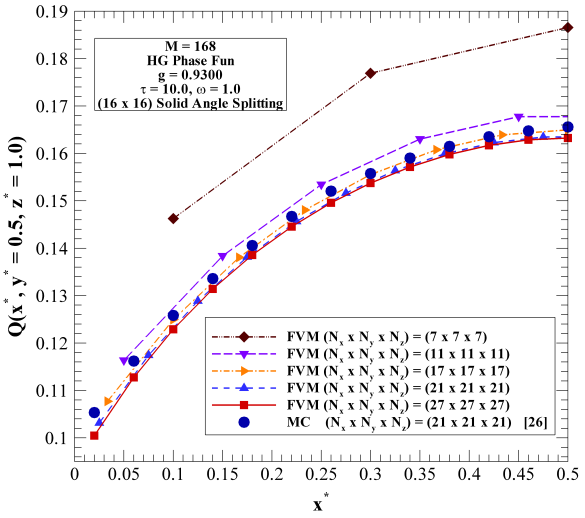

Figure 3: Impact of spatial grid density on Q(x*, y* = 0.5, z* = 1) for diffuse heating at z* = 0 wall generated using FVM with M = 168 discrete directions for g = 0.9300 and comparison with Monte Carlo solutions [26]

Figure 4 examines the impact of phase-function normalization on $Q(x^*, y^* = 0.5, z^* = 1.0)$ for three different HG asymmetry factors: g = 0.2000, 0.8000, and 0.9300. Profiles generated via the FVM using either Hunter and Guo's normalization technique or no normalization with sufficient solid-angle splitting are compared to reference MC results [26] to gauge their accuracy. The profiles were generated using M = 168 discrete directions, and thus solid-angle splitting of $(N_{s\phi}$ x $N_{s\theta})$ = (16 x 16) is implemented to ensure accurate scattered energy conservation.

For weakly-forward scattering (g = 0.2000), FVM profiles both with and without phase-function normalization produce nearly identical results. When normalization is not applied, the discretized g is altered from 0.2000 to 0.1975, indicating that asymmetry factor is not exactly conserved. However, according to the isotropic scaling law, this alteration corresponds to a change in scattering effect of just 0.2%, explaining why this change in g doesn't produce significant error. This result also conforms to the findings of Hunter and Guo for normalization using the DOM, in which the impact of normalization was minimal for weakly-forward scattering.

As asymmetry factor is increased, differences between the normalized and non-normalized heat flux profiles begin to appear. For a prescribed g = 0.8000, non-normalization alters the discretized value to g = 0.7900, leading to a 5% change in scattering effect. For the highly anisotropic case, the discretized g is altered from 0.9300 to 0.9198 (14.6% scattering effect change). The difference between non-

normalized and normalized heat flux ranges between -7.42% near $x^* = 0$ to -4.59% at the center of the face. Additionally, when compared to MC predictions, it is seen that heat flux generated using Hunter and Guo's normalization technique conforms more accurately than when normalization is ignored. Without normalization, the FVM profile underpredicts the MC by between 5.69% and 11.7% over the range of x^*. Conversely, when Hunter and Guo's technique is applied to conserve the original asymmetry factor, the FVM profile underpredicts by less than 2% for all locations except near $x^* = 0$, where the maximum difference reaches 4.62%.

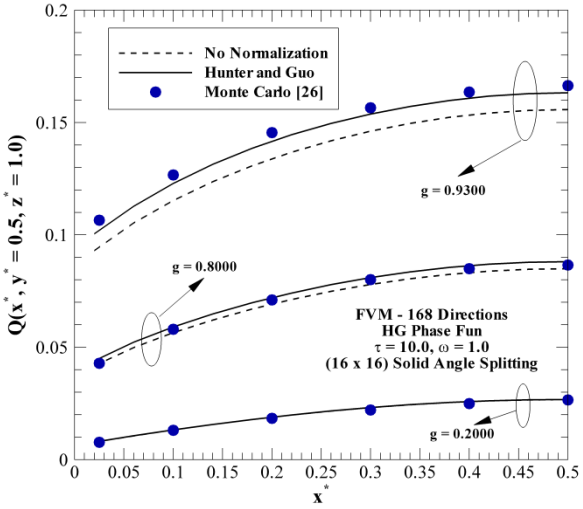

Figure 4: Impact of diffuse normalization on Q(x*, y* = 0.5, z* = 1) for diffuse heating at z* = 0 wall generated using FVM with M = 168 discrete directions for g = 0.9300 and comparison with Monte Carlo solutions [26]

Figure 5 investigates the impact of angular discretization (i.e., the number of discrete directions) on both normalized and non-normalized FVM heat flux in a highly-anisotropic medium with $g = 0.9300$. Reference MC values are also plotted, for comparison. When normalization is not implemented, heat flux profiles generated for all directional numbers underpredict MC solutions significantly, with maximum differences of 37.0%, 26.8%, 19.5%, and 11.71% witnessed for $M = 24$, 48, 80, and 168 directions, respectively. The average percent differences for the same direction numbers are 27.0%, 20.2%, 13.7%, and 7.11%. As expected, increase in discrete direction number does decrease the difference with respect to MC. When Hunter and Guo's normalization is applied, the percentage differences are decreased for all quadratures except the lowest order ($M = 24$). For $M = 48$, 80, and 168, the maximum differences are 8.07%, 7.51%, and 4.62%, with average differences of 4.01%, 4.09%, and 1.79%, respectively. For the lowest order quadrature, FVM heat flux profiles conform accurately to MC near $x^* = 0$ (differences of less than 2.0%), but differ by nearly 30% near the wall center.

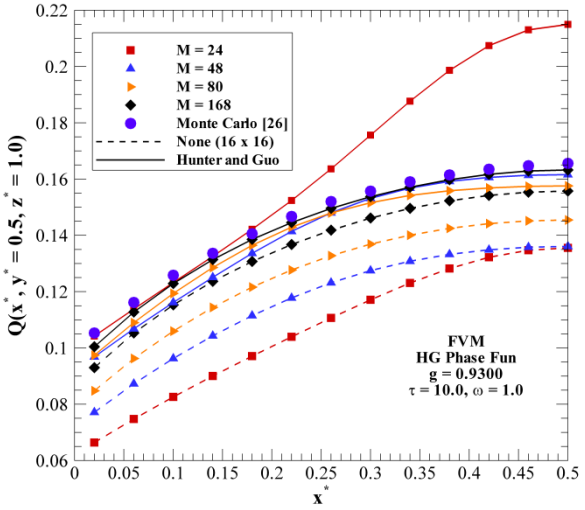

Figure 5: Impact of discrete direction number on Q(x*, y* = 0.5, z* = 1) for diffuse heating at z* = 0 and comparison with Monte Carlo results [26] for g = 0.9300

The underlying cause of this large discrepancy near the wall can be found by examining the values of discretized phase function for this directional order. Figure 6a plots discretized phase function values vs. the cosine of scattering angle both with and without phase-function normalization for $M = 24$, and compares them with the theoretical HG phase function values calculated using Eq. (10). When normalization is not applied, the phase-function values do not conform accurately to the theoretical phase function. As scattering cosine increases, large bumps in the discretized phase-function profile are witnessed. Without normalization, the discretized asymmetry factor is altered to 0.8866, corresponding to a 62% change in scattering effect.

After application of Hunter and Guo's technique, asymmetry factor is effectively conserved. However, the discretized values of scattering phase function still exhibit significant differences from the theoretical phase function, especially as scattering cosine approaches unity. The minimal amount of discrete directions in this quadrature isn't able to accurately represent the true nature of the theoretical phase function shape, even though the asymmetry factor is accurately conserved. In contrast, when a larger number of discrete directions is implemented ($M = 168$) in Figure 4b, application of Hunter and Guo's normalization results in both conserved asymmetry factor and an accurate representation of phase-function shape. Thus, the attained shape of the discretized phase-function values is of extreme importance when a minimal number of discrete radiation directions are used for simulation.

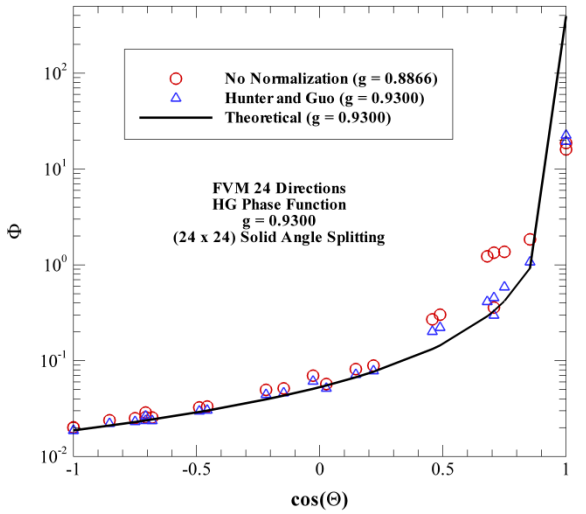

(a)

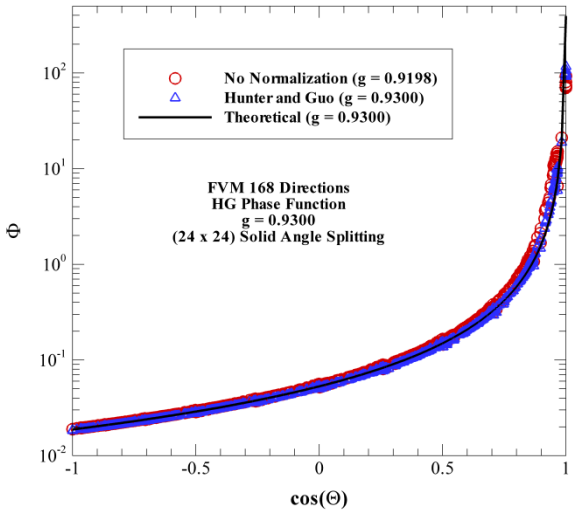

(b)

Figure 6: Comparison of discretized HG phase-function values vs. cosine of scattering angle with prescribed g = 0.9300 both with and without phase-function normalization using FVM with a) M = 24 and b) M = 168 discrete directions

A comparison of heat flux values $Q(x^*, y^* = 0.5, z^* = 1.0)$ generated using the FVM with $M = 168$ directions both with and without phase-function normalization to both MC [26] and DOM S_{12} [30] results are presented in Table 1. In essence, radiative transfer results for a given problem should be independent of the solution method implemented. Thus, comparisons to DOM and MC results will bolster confidence that the generated FVM results are accurate. DOM results generated by Hunter and Guo [30] are presented for two normalization cases: normalization to conserve scattered energy only, i.e. Eq. (9), and using Hunter and Guo's technique. One disadvantage of the DOM is that there is no way to implement an analogous solid-angle splitting technique to conserve scattered energy, so phase-function normalization is almost always required for anisotropic scattering to obtain a convergent solution. Simulation parameters, such as optical properties and grid density, are listed in the table footnotes.

Table 1: Comparison of $Q(x^*, y^* = 0.5, z^* = 1.0)$[a,b] values generated using DOM[c] [30] and FVM[d] with various normalization techniques to reference MC values [26]

x/L	MC [22]	DOM [25]		MC [22]	FVM	
		Energy Norm.	Hunter and Guo		No Norm.	Hunter and Guo
		g = 0.9735	g = 0.9300		g = 0.9198	g = 0.9300
0.02	0.1053	0.1496	0.0988	0.1053	0.0930	0.1005
0.10	0.1258	0.1659	0.1182	0.1258	0.1153	0.1229
0.14	0.1336	0.1779	0.1268	0.1336	0.1237	0.1314
0.22	0.1467	0.2010	0.1409	0.1467	0.1368	0.1446
0.30	0.1557	0.2126	0.1497	0.1557	0.1461	0.1537
0.38	0.1615	0.2147	0.1543	0.1615	0.1523	0.1598
0.42	0.1635	0.2144	0.1555	0.1635	0.1542	0.1617
0.50	0.1656	0.2139	0.1565	0.1656	0.1558	0.1633

[a] Optical thickness $\tau = 10.0$, scattering albedo $\omega = 1.0$, HG phase-function with $g = 0.9300$

[b] $(N_x \text{ x } N_y \text{ x } N_z) = (27 \text{ x } 27 \text{ x } 27)$ for FVM and DOM

[c] DOM generated using S_{12} quadrature

[d] FVM with $M = 168$ using FT_N-FVM quadrature, $(N_{s\phi} \text{x } N_{s\theta}) = (24 \text{ x } 24)$ solid-angle splitting

At all locations, heat fluxes generated using the DOM S_{12} with scattered energy normalization greatly overpredict MC values, due to an alteration of the prescribed asymmetry factor from $g = 0.9300$ to 0.9735, yielding an increase in scattering effect of 62.0%. Correspondingly, DOM heat fluxes overpredict by a maximum of 42.0% and an average of 34.2%. Application of Hunter and Guo's technique reduces the error, with DOM heat flux underpredicting the MC results by a maximum of 6.23% and an average of 5.15%, respectively.

The ability to use solid-angle splitting to conserve scattered energy in the FVM results in a smaller discrepancy in discretized asymmetry factor than for the DOM. When normalization is ignored, sufficient solid-angle splitting produces a discretized $g = 0.9198$, as opposed to $g = 0.9735$ for DOM with scattered energy normalization. As previously mentioned in the discussion of Figure 4, the FVM profile without normalization underpredicts the MC results by a maximum and average of 11.70% and 7.22%, respectively. Application of Hunter and Guo's technique reduces these underpredictions to 4.62% and 1.87%, respectively. In general, FVM profiles tend to be more accurate in comparison

with MC than the corresponding DOM profiles. The average difference between DOM and FVM heat flux profiles is 44.8% when asymmetry factor conservation is ignored. Due to the relative similarity of the two methods, a difference of this magnitude between FVM and DOM is inordinately large. Application of Hunter and Guo's technique for both numerical methods reduces the average difference to 3.19%. The accurate conformity of the normalized FVM profile to both normalized DOM and MC results gives confidence that scattering properties of the medium are being accurately conserved through proper phase-function normalization.

The impact of solid-angle splitting on radiative transfer results generated using the FVM both with and without normalization is examined in Figures 7(a-b), in which percentage differences between FVM heat fluxes and reference MC results are plotted for various levels of solid-angle splitting. Percentage differences are presented for $M = 80$ directions in Figure 7a, and for $M = 288$ directions in Figure 7b. When no normalization is applied, increases in the solid-angle splitting density result in convergence of FVM heat flux profiles to values that underpredict the MC significantly at all locations x^*. As discussed in the results shown in Fig. 1, solid-angle splitting of $(N_{s\phi} \times N_{s\theta}) = (20 \times 20)$ and (12×12) are required to accurately conserve scattered energy within 0.001% for $M = 80$ and 288, respectively. The results in Figs. 7(a-b) reflect the previous results, as convergence of the percentage differences occurs around these levels of splitting. For $M = 80$, solid-angle splitting of $(N_{s\phi} \times N_{s\theta}) = (20 \times 20)$ results in percentage differences ranging between 11.8% and 19.7% when normalization is not applied. Similarly, for $M = 288$, splitting of $(N_{s\phi} \times N_{s\theta}) = (12 \times 12)$ results in the FVM profiles underpredicting MC results by between 3.76% and 8.26%, depending on location. Increase in direction number does improve FVM predictions in comparison with FVM, however the lack of asymmetry factor conservation and resulting angular false-scattering errors still result in significant differences between FVM and MC results.

In both Figure 7a and 7b, percentage differences between FVM using Hunter and Guo's normalization with splitting levels of $(N_{s\phi} \times N_{s\theta}) = (2 \times 2)$ and (24×24) are also presented. For both directional quadratures, use of Hunter and Guo's technique significantly reduces discrepancies between FVM and MC results. Differences between MC and FVM profiles using Hunter and Guo's technique are less than 7.5% at all locations for $M = 80$, and less than 3.7% for all locations for $M = 288$. Of greater importance, however, is the fact that profiles generated with both low and high solid-angle splitting densities produce nearly identical FVM heat flux profiles. The maximum percent difference between FVM profiles generated with $(N_{s\phi} \times N_{s\theta}) = (2 \times 2)$ and (24×24) solid-angle splitting is 0.35% and 0.20% for $M = 80$ and 288, respectively, indicating that further solid-angle splitting past $(N_{s\phi} \times N_{s\theta}) = (2 \times 2)$ is not required to obtain more accurate radiative transfer solutions when implementing Hunter and Guo's normalization technique.

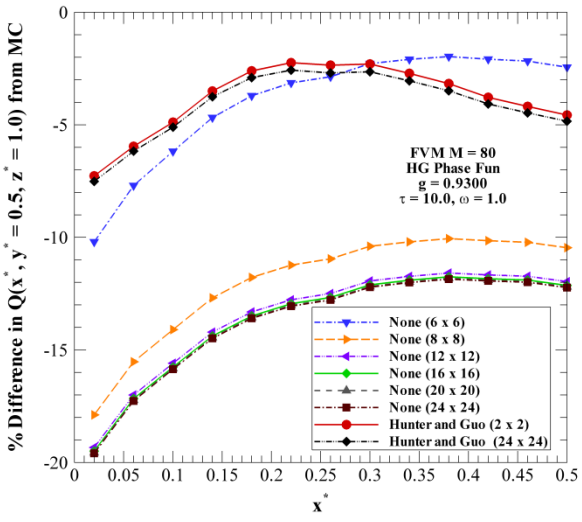

(a)

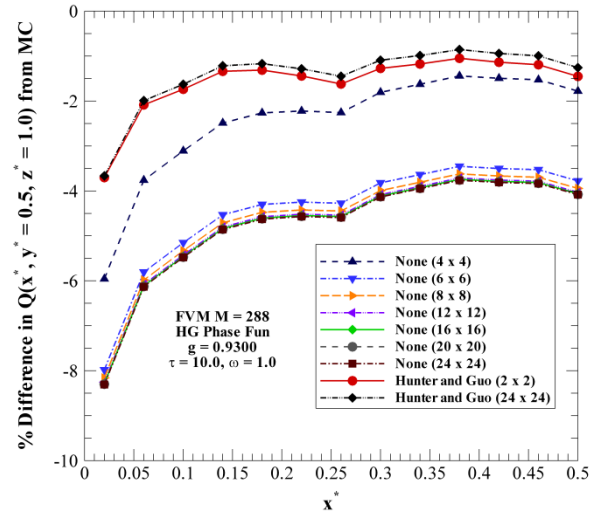

(b)

Figure 7: Percent difference in Q(x*, y* = 0.5, z* = 1) between MC solution [26] and FVM solutions both with and without phase-function normalization using various solid angle splitting densities for a) M = 80 and b) M = 288 discrete directions

The ability to produce accurate FVM solutions with respect to MC with minimal solid angle splitting has a distinct advantage when it comes to computational convergence time. FVM convergence times for varying number of discrete directions and various solid angle splitting levels are presented in Table 2 for the problem analyzed in Figure 5 (optically thick, purely scattering medium with $g = 0.9300$). Computational times using splitting levels ranging from $(N_{s\phi} \times N_{s\theta}) = (2 \times 2)$ to (24×24) for the non-normalized case are presented, as well as the computational time for Hunter and Guo's normalization

with $(N_{s\phi} \times N_{s\theta})$ = (2 x 2) splitting, as the results from Figures 7(a-b) show that further refinement is unnecessary.

When normalization is not applied, the use of $(N_{s\phi} \times N_{s\theta})$ = (2 x 2) solid angle splitting results in divergent radiative transfer solutions for all directional quadratures except M = 288, corresponding to the lack of scattered energy conservation seen for this splitting level in Figure 1. As splitting is increased, and scattered energy is more effectively conserved, computational times initially start to decrease slightly from values at lower splitting levels. Eventually, as the splitting becomes more greatly refined, computational times drastically increase. For M = 288, increasing splitting level from (4 x 4) to (24 x 24) results in a 406% increase in computational time. Use of Hunter and Guo's normalization allows for convergence and accuracy with just (2 x 2) splitting, greatly reducing convergence times. According to the results of Figure 1, splitting of at least $(N_{s\phi} \times N_{s\theta})$ = (24 x 24), (20 x 20), (20 x 20), (12 x 12), and (12 x 12) are required to accurately conserve scattered energy within 0.001% when normalization is not implemented. Use of these splitting levels results in computational times that are 3.51, 2.96, 3.06, 1.22, and 1.26 times higher than the convergence times using Hunter and Guo's normalization with (2 x 2) solid angle splitting. This indicates that Hunter and Guo's technique allows for more accurate solutions when compared to MC, providing an indication of the importance of accurately conserving phase-function asymmetry factor for FVM predictions.

Based on the trend in asymmetry factor conservation seen in Figure 2, further increase in discrete direction number past M = 288 should reduce the discrepancy between discretized and prescribed asymmetry factor for high solid-angle splitting without phase-function normalization. It therefore is possible that, with a sufficient number of discrete directions, that scattered energy and asymmetry factor could be accurately conserved without additional phase-function normalization. This is investigated in Figure 8, wherein FVM heat fluxes generated using M = 624, 1088, and 2024 discrete directions without the use of phase-function normalization are plotted versus wall location x^*. As a comparison, both reference MC solutions and FVM solutions with Hunter and Guo's technique at lower direction number (M = 168 and 288) are also plotted in Figure 8.

Increasing discrete direction number to M = 624, 1088, and 2024 results in discretized asymmetry factors of g = 0.9270, 0.9282, and 0.9290, respectively, showing that direction increase will reduce the change in scattering effect. When corresponding FVM heat fluxes are compared to MC, it is seen that an increase in directions when normalization is ignored does reduces angular false scattering error. The average percentage differences for the three extreme direction numbers are 3.00%, 2.43%, and 2.17%, respectively. Further increase in direction past M = 2024 would reduce the discrepancy in discretized asymmetry factor further, corresponding to more accurate results. However, increases of this magnitude in discrete direction number correspond to drastic increases in computational convergence times. The three profiles corresponding to the previously mentioned direction numbers took 5650, 16520, and 65400 seconds to converge, respectively. In addition, it is seen in Figure 8 that the M = 168 and 288 FVM profiles generated using Hunter and Guo's normalization are more accurate than these extreme direction cases, with average differences of only 1.82% and 1.58%, respectively. These two profiles with said accuracy can be generated, using (2 x 2) splitting, in 497 and 1341 seconds, respectively, indicating that use of Hunter and Guo's technique is both more efficient and more accurate than these higher direction cases.

Table 2: Computational convergence times, in seconds, for FVM with and without normalization at various solid-angle splitting levels and varying number of directions

$(N_{s\phi} \times N_{s\theta})$ / M	No Normalization (sec)								New Norm (sec)
	(2 x 2)	(4 x 4)	(6 x 6)	(8 x 8)	(12 x 12)	(16 x 16)	(20 x 20)	(24 x 24)	(2 x 2)
24	Diverge	Diverge	21.37	14.70	15.38	20.76	33.03	50.86	14.51
48	Diverge	75.21	50.00	47.21	54.40	77.532	124.0	207.0	41.84
80	Diverge	116.5	110.6	113.0	141.8	203.9	335.9	556.6	109.8
168	Diverge	531.0	491.5	514.1	606.7	834.2	1415	2414	497.0
288	1538	1385	1340	1438	1687	2438	4133	7011	1341

Figure 9 plots FVM heat fluxes, generated with and without normalization, in an optically thin (τ = 1.0), purely scattering medium with g = 0.9300 in order to gauge the impact of optical thickness. MC results taken from Boulet et al. [26] are also presented in Figure 9. For the three direction numbers presented (M = 48, 80, and 168), the difference between non-normalized and normalized FVM heat fluxes is minimal. The largest differences for these three direction numbers are 3.35%, 1.41%, and 0.82%, respectively. For an optically thin medium, radiative energy is able to penetrate a much larger distance into the medium before scattering. Therefore, many fewer scattering events occur as compared to the optically thick medium described in the rest of the analysis,

and the distortions in asymmetry factor when normalization is not applied do not have as strong of an impact.

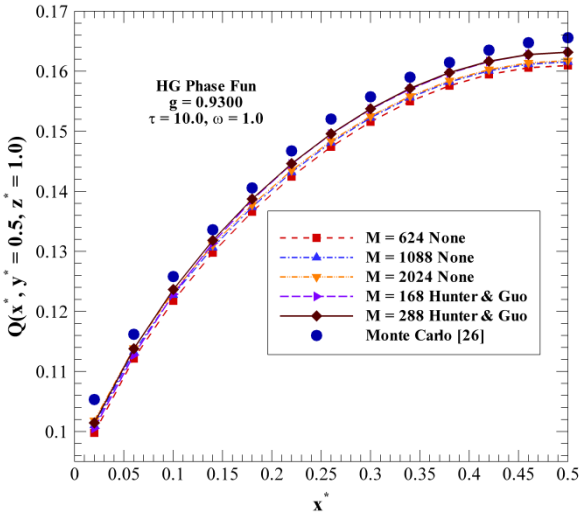

Figure 8: Comparison of Q(x*, y* = 0.5, z* = 1.0) for diffuse heating at z* = 0 wall between MC solutions [26] and FVM solutions using extremely high-order quadrature

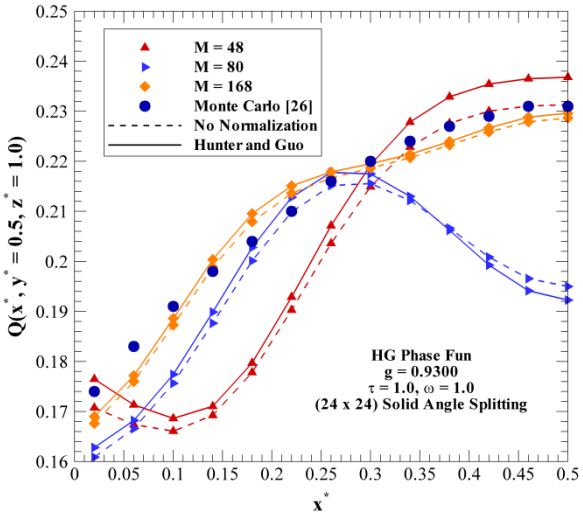

Figure 9: Impact of discrete direction number on Q(x*, y* = 0.5, z* = 1) for diffuse heating at z* = 0 and comparison with Monte Carlo results [26] for g = 0.9300 in an optically thinner medium

In addition, the FVM heat flux profiles exhibit different behavior and shape than the reference MC values. Physically impossible bumps in the heat flux profiles appear due to ray effect [35], an error based on angular discretization that has been shown to be prominent for optically thin media. For M = 168, the percentage differences between MC and FVM with Hunter and Guo's normalization ranges from a 3.20% underprediction at x^* = 0.06 to a 2.72% overprediction at x^* = 0.18. Thus, while Hunter and Guo's technique minimizes errors due to a lack of asymmetry factor conservation, ray effect is still prominent for simulation in optically thin media.

CONCLUSIONS

In this study, the impact of angular false scattering errors due to a lack of asymmetry factor conservation in FVM radiative transfer analysis is examined, and the necessity of proper phase-function normalization to produce accurate radiative transfer predictions is discussed. The following conclusions can be made from this study:

(1) The commonly implemented technique of solid-angle splitting for the FVM phase function treatment is able to accurately conserve scattered energy in the system, provided that a sufficient splitting density is used. However, it still may not be able to conserve the phase-function asymmetry factor simultaneously, leading to changes in scattering effect after discretization.

(2) For weakly-anisotropic media, results obtained using the FVM without normalization and with Hunter and Guo's normalization technique to accurately conserve asymmetry factor are minimally different, corresponding to expectations found in DOM radiative transfer analysis. This is due to the change in scattering effect, manifested in the difference in $(1 - g)$, being small for weakly-forward scattering.

(3) When scattering is highly anisotropic, small deviations in asymmetry factor after discretization without normalization result in significant discrepancies in FVM heat flux when compared to reference MC results.

(4) Application of Hunter and Guo's normalization technique eliminates errors in discretized asymmetry factor as well as energy, and produces FVM heat fluxes that are more accurate to MC predictions than when normalization is ignored. Normalized FVM results also compare accurately to previously published normalized DOM results, giving confidence that the generated heat fluxes are accurate and that angular false scattering errors are reduced. Hunter and Guo's technique also greatly reduces computational convergence times, since large solid angle splitting is not required for accurate solutions.

(5) For optically thin media, the impact of discretized asymmetry factor conservation is minimal, due to the lack of scattering events. Additionally, ray effect is prevalent, causing unrealistic heat flux profiles.

(6) While sufficient increases in discrete direction number can reduce/minimize angular false scattering in FVM, Hunter and Guo's normalization technique is a more efficient method to improve treatment of anisotropic scattering in radiative transfer, as extreme refinement of angular grid and solid-angle splitting are not required. This is of paramount importance and reality in the practice of 3-D radiative heat transfer computations.

REFERENCES

[1] Modest, M.F., *Radiative Heat Transfer*, *2nd ed.,* Academic Press, New York, 2003, pp. 263-284, 498-530.

[2] Siegel, R., Howell, J.P., *Thermal Radiation Heat Transfer, 4th ed*., Taylor and Francis, New York, 2002, pp. 371-490.

[3] Solovjov, V.P., Webb, B.W., An efficient method for modeling radiative transfer in multicomponent gas mixtures with soot, J. Heat Transfer, 2001, 123:450-457.

[4] Borjini, M.N., Guedri, K., Said, R., Modeling of radiative heat transfer in 3D complex boiler with non-gray sooting media, J. Quant. Spectrosc. Radiat. Transfer, 2007, 105:167-179.

[5] Tuncer, O., Acharya, S., Uhm, J.H., Dynamics, NOx and flashback characteristics of confined premixed hydrogen-enriched methane flames, Int. J. Hydrogen Energy, 2009, 34:496-506.

[6] Guo, Z., Maruyama, S., Radiative heat transfer in nonhomogeneous, nongray, and anisotropic scattering media, Int. J. Heat Mass Transfer, 2000, 43:2325-2336.

[7] Guo, Z., Maruyama, S., Tagawa, S., Combined heat transfer in floating growth of large silicon crystals with radiation on diffuse and specular surfaces, J. Crystal Growth, 1998,194:321-330.

[8] Kim, K.H., Guo, Z., Ultrafast radiation heat transfer in laser tissue welding and soldering, Num. Heat Transfer A, 2004, 46:23-40.

[9] Kim, K.H., Guo, Z., Multi-time-scale heat transfer modeling of turbid tissues exposed to short-pulsed irradiations, Comp. Meth. Prog. Bio., 2007, 86:112-123.

[10] Jaunich M., Raje, S., Kim, K.H., Mitra, K., Guo, Z., Bio-heat transfer analysis during short pulse laser irradiation of tissues, Int. J. Heat Mass Transfer, 2008, 51:5511-5521.

[11] Raithby, G.D., Chui, E.H., A finite-volume method for predicting a radiant heat transfer in enclosures with participating media, J. Heat Transfer, 1990, 112 (1):415-423.

[12] Chui, E.H., Raithby, G.D., Hughes, P.M.J., Prediction of radiative transfer in cylindrical enclosures with the finite volume method, J. Thermophys. Heat Transfer, 1992, 6:605-611.

[13] Chui, E.H., Raithby, G.D., Computation of radiant heat transfer on a nonorthogonal mesh using the finite-volume method, Num. Heat Transfer B, 1993, 23 (3):269-288.

[14] Chui, E.H., Hughes, P.M.J., Raithby, G.D., Implementation of the finite-volume method for calculating radiative-transfer in a pulverized fuel flame, Combust. Sci. Tech., 1993, 92:225-242.

[15] Murthy, J.Y., Mathur, S.R., Finite volume method for radiative heat transfer using unstructured meshes, J. Thermophys. Heat Transfer, 1998, 12(3):313-321.

[16] Kim, M.Y., Baek, S.W., Park, J.H., Unstructured finite-volume method for radiative heat transfer in a complex two-dimensional geometry with obstacles, Num. Heat Transfer B, 2001, 39:617-635.

[17] Chai, J.C., Lee, H.S., Patankar, S.V., Finite volume method for radiation heat transfer, J. Thermophys. Heat Transfer, 1994, 8(3):419-425.

[18] Raithby, G.D., Discussion of the finite-volume method for radiation, and its application using 3D unstructured meshes, Num. Heat Transfer B, 1999, 35(4):389-405.

[19] Baek, S.W., Kim, M.Y., Kim, J.S., Nonorthogonal finite-volume solutions of radiative heat transfer in a three-dimensional enclosure, Num. Heat Transfer B, 1998, 34(4):419-437.

[20] Seung, H., Huh, K.Y., Assessment of the finite-volume method and the discrete ordinate-method for radiative heat transfer in a three-dimensional rectangular enclosure, Num. Heat Transfer B, 1999, 35(1):85-112.

[21] Chai, J.C., Hsu, P.-f., Lam, Y.C., Three-dimensional transient radiative transfer modeling using the finite-volume method, J. Quant. Spectrosc. Radiat. Transfer, 2004, 86(3):299-313.

[22] Guo, Z., Kumar, S., Three-dimensional discrete ordinates in transient radiative transfer, J. Thermophys. Heat Transfer, 2002, 16:289-296.

[23] Kim, S.H., Huh, K.Y., A new angular discretization scheme of the finite volume method for 3-D radiative heat transfer in absorbing, emitting, and anisotropically scattering media, Int. J. Heat Mass Transfer, 2000, 43:1233-1242.

[24] Kamel, G., Naceur, B.M., Rachid, M., Rachid, S., Formulation and testing of the FTn finite volume method for radiation in 3-D complex inhomogeneous participating media, J. Quant. Spectrosc. Radiat. Transfer, 2006, 98:425-445.

[25] Kim, T.K., Lee, H., Effect of anisotropic scattering on radiative heat transfer in two-dimensional rectangular enclosures, Int. J. Heat Mass Transfer, 1988, 31:1711-1721.

[26] Boulet, P., Collin, A., Consalvi, J.L., On the finite volume method and the discrete ordinates method regarding radiative heat transfer in acute forward anisotropic scattering media, J. Quant. Spectrosc. Radiat. Transfer, 2007, 104(1):460-473.

[27] Hunter, B., Guo, Z., Conservation of asymmetry factor in phase function discretization for radiative transfer analysis in anisotropic scattering media, Int. J. Heat Mass Transfer, 2012, 55:1544-1552.

[28] Hunter, B., Guo, Z., Phase function normalization for accurate analysis of ultrafast collimated radiative transfer. Appl. Optics, 2012, 51:2192-2201.

[29] Hunter, B., Guo, Z., Phase-function normalization in 3-D discrete-ordinates solution of radiative transfer – Part I: Conservation of scattered energy and asymmetry factor, Num. Heat Transfer B. 2012, 62:203-222.

[30] Hunter, B., Guo, Z., Phase-function normalization in 3-D discrete-ordinates solution of radiative transfer – Part II: Benchmark comparisons, Num. Heat Transfer B, 2012, 62:223-242.

[31] Hunter, B., Guo, Z., Reduction of angle splitting and computational time for the finite volume method via phase function normalization, Int. J. Heat Mass Transfer, 2012, 55:2449-2460.

[32] Hunter, B., Guo, Z., Comparison of discrete-ordinates method and finite volume method for steady-state and ultrafast radiative transfer analysis in cylindrical coordinates, Num. Heat Transfer B, 2011, 59:339-359.

[33] Guo, Z., Maruyama, S., Scaling anisotropic scattering in radiative transfer in three-dimensional nonhomogeneous media, Int. Comm. Heat Mass Transfer, 1999, 26:997-1007.

[34] Guo, Z., Kumar, S., Equivalent isotropic scattering formulation for transient short-pulse radiative transfer in anisotropic scattering planar media, Appl. Optics, 1999, 39(24):4411-4417

[35] Chai, J.C., Lee, H.S., Patankar, S.V., Ray effect and false scattering in the discrete ordinates method, Num. Heat Transfer B, 1993, 24:373-389.